Nanocrystalline Ni Coatings Strengthened with Ultrafine Particles

JIANHONG HE and JULIE M. SCHOENUNG

In this study, nanocrystalline Ni powders and thermally sprayed coatings, containing ultrafine AlN particles, were synthesized and characterized. The results indicated that the presence of AlN particles in the powders drastically decreased the dimension of agglomerates formed by cryomilling and increased the surface roughness of the agglomerates. The AlN phase was broken down into ultrafine particles of approximately 30 nm in size. These particles were dispersed in the Ni matrix and enhanced the development of a nanocrystalline structure in the Ni matrix during cryomilling. Selected-area diffraction patterns, obtained from transmission electron microscopy (TEM) and X-ray mapping with scanning electron microscopy (SEM), confirmed the presence of AlN particles in the coatings. The presence of AlN particles also led to an increase in the amount of NiO phase that was distributed in the coating, in the form of ultrafine, round particles. AlN particles increased the microhardness of the Ni coating by approximately 60 pct. Indentation-fracture results also indicated that the fine, dispersed AlN particles raised the apparent toughness of the Ni coating. The synthesized Ni coatings containing ultrafine AlN particles were characterized as equiaxed nanocrystalline grains with an average size of 24 nm, in which twins were observed. The increase in microhardness resulted from both grain refinement and the presence of ultrafine particles. The latter played the primary role in strengthening.

I. INTRODUCTION

THE significant performance enhancement that results from the presence of small amounts of dispersed fine particles in materials is well recognized, *i.e.*, improving strength through interactions with deformation faults[1,2,3] and inhibiting grain growth due to Zener pinning.[4,5] The contributions of nitrides and oxides (formed through reactions between powders and oxygen/nitrogen from the environment during mechanical milling in liquid nitrogen) to the thermal stability of nanocrystalline materials have been realized.[6–9] Strengthening has also been found to result from the presence of ultrafine precipitates in nanostructured coatings.[10,11] Mechanical milling in liquid nitrogen has been employed to synthesize nanocrystalline Ni powders, which can be used as feedstock powders to fabricate nanocrystalline Ni coatings.[12] However, Ni does not form a stable nitride in the nitrogen atmosphere. In principle, the nitrogen atmosphere could result in the formation of hexagonal Ni_3N ($a = 2.670$ Å and $c = 4.306$ Å), but the formation enthalpy of Ni_3N at room temperature is quite low ($\Delta H_{298} = 0.8$ kJ/mol[13]), indicating its instability at room temperature. Alternatively, the high hardness and thermal stability of aluminum nitride, (AlN) are well known.[14,15] Therefore, the aim of the present study was to demonstrate another method for introducing the nitride phase, namely, through the intentional addition of AlN to the milling process, and to provide insight into the influence of these AlN particles on the microstructural evolution and mechanical properties of nanocrystalline Ni/AlN coatings. Furthermore, we demonstrate that the AlN additions need not be in the nanometer scale at the start. They fracture during milling to become finely dispersed in the Ni matrix, in much the same way as a nitride created during milling.

II. EXPERIMENTAL PROCEDURE

Commercially available, pure Ni powder (Sulzer Metco Inc., Westbury, NY) with a purity ≥99.5 wt pct and a nominal particle size of 45 ± 11 μm and AlN powder (CERAC Inc., Milwaukee, WI) with a purity of 99 pct and a nominal particle size of 1.97 μm were selected for the present study. The Ni powders were blended with AlN powders for 0.5 hours in the amounts of 0, 0.5, and 2 wt pct AlN (or 0, 1.38, and 5.54 vol pct AlN, using specific-gravity values of 3.26[14,15] and 8.902[16] g/cm^3 for AlN and Ni, respectively). The blended powders were mechanically milled in a modified Union Process 1-S attritor mill with a grinding-tank capacity of 0.0057 m^3. Stainless steel balls of 0.635 cm in diameter were used, with a powder-to-ball mass ratio of 1:20. The powder charge was 1 kg. The mill was operated at 180 r.p.m. for 8 hours, and liquid nitrogen was continuously introduced into the attritor tank. The flux of liquid nitrogen was properly controlled using a valve, so that the milling temperature, monitored by a thermocouple, was maintained at a relatively constant value of 100 K.

On the basis of ASTM E1019 and ASTM E1097 standards, chemical analysis of the as-received and cryomilled powders was conducted by Luvak Inc., a professional chemical-analysis company located in Boylston, MA. The particle size and distribution were determined using a particle analyzer made by Coulter Co. (Miami, FL).

Thermal spraying of the powders was carried out by using a Sulzer Metco (Westbury, NY) DJ 2600 high-velocity oxy-fuel (HVOF) spray system on carbon steel (0.2 wt pct C) substrates that were located at a distance of 0.230 m away

JIANHONG HE, Materials Scientist, and JULIE M. SCHOENUNG, Professor, are with the Department of Chemical Engineering and Materials Science, University of California, Davis, Davis, CA 95616-5294. Contact e-mail:jmschoenung@ucdavis.edu

Manuscript submitted January 10, 2002.

Table I. Spraying Parameters Used to Produce Ni with Aluminum Nitride Coatings

Gas	Pressure (MPa)	FMR*	GSF**	Parameters	Setting
Air	0.69	40	5616	powder feed rate	0.315 g/s
Propylene	0.69	43	1488	X-Y traverse speed	1.1016 m/s
Oxygen	1.034	30	3410	spraying distance	0.230 m

*FMR = flow meter reading.
**GSF = gas standard flow (mm^3/s).

from the nozzle of the spray gun. Before spraying, the surface of the substrate was grit blasted with abrasive Al_2O_3 particles to create a superficial roughness, which improves the bonding strength between the coating and the substrate. The spray facility and process are described in detail elsewhere,[17,18] and the spray parameters are listed in Table I. Four categories of coatings were produced using the following powders: (1) the as-received Ni powders; (2) the cryomilled Ni powders; (3) the cryomilled (Ni + 0.5 wt pct AlN) powders; and (4) the cryomilled (Ni + 2 wt pct AlN) powders. The corresponding coatings are referred to in this manuscript as the conventional Ni coating, the cryo Ni coating, the cryo (Ni + 0.5 wt pct AlN) coating, and the cryo (Ni + 2 wt pct AlN) coating. Five spray passes were performed for each coating.

The X-ray diffraction (XRD) measurements were performed in the 2θ range from 30 to 100 deg using Cu K_α (λ = 0.15418 nm) radiation in a Siemens (Erlangen, Germany) D5000 diffractometer equipped with a graphite monochromator. A low scanning rate of scans, with a step size of 0.01 deg and a step time of 5 seconds, was used to assure the detection of reflections from second phases with low percentages. After the effects of K_{α_2} were corrected, the peak position and full-width at half-maximum of the XRD reflections of Ni were computed using a software package in the Siemens D5000 diffractometer. In the present work, the fully annealed Ni powder was used as a standard sample for the determination of instrumental broadening. Scanning electron microscopy (SEM) observations were performed on a PHILIPS* XL 30 microscope with a field-emission gun.

*PHILIPS is a trademark of Philips Electronic Instruments Corp., Mahwah, NJ.

Transmission electron microscopy (TEM) studies were conducted on a PHILIPS CM microscope operated at 200 keV; the preparation of powder samples is described in detail elsewhere,[19] and the coating samples were prepared using a standard grinding-dimpling–ion milling procedure. The microhardness of the cross section of the coatings was tested, and indentation cracking was examined using a Buehler (Lake Bluff, IL) Micromet 2004 microhardness tester.

III. RESULTS AND DISCUSSION

A. *Powder Characteristics*

The SEM secondary electron images in Figures 1(a) through (d) show morphological differences among the as-received Ni powder (Figure 1(a)), the cryomilled Ni powder (Figure 1(b)), and the cryomilled (Ni + AlN) powders (Figures 1(c) and (d)). As a result of cryomilling, spherical Ni powders were transformed into irregular, flake-shaped agglomerates. Compared to the smooth and well-defined agglomerate external surfaces of the cryomilled Ni powder (Figure 1(b)), the agglomerate external surfaces of the cryomilled (Ni + 0.5 wt pct AlN) powder became rougher due to interaction with the hard particles (Figure 1(c)). An increase in the amount of hard particles to 2 wt pct led to agglomerates breaking down into small, ragged fragments. The boundaries to these ragged fragments are difficult to distinguish (Figure 1(d)), which is a common morphological feature of mechanically milled composite powders.[17,20,21] Observation with high-resolution SEM has indicated that such agglomerates still consist of very fine particles.[20] It is noted that in the present cryomilled (Ni + 2 wt pct AlN) powder, a few uncrushed agglomerates are also seen, as indicated by the arrows in Figure 1(d).

Figure 2 shows the distribution of powder particle/agglomerate size for the different powders. The as-received Ni powder had a narrow size range with a median of 41 μm, consistent with their nominal particle size of 45 ± 11 μm. Cryomilling increased the median size to 53 μm and broadened the range of the size distribution. The increase in agglomerate size caused by cryomilling has also been observed in other fcc materials.[22] The addition of hard particles led to a decrease in the average agglomerate size and an increase in the range of the size distribution, compared with cryomilled Ni powder. Consistent with the SEM morphological images, the median agglomerate size of the cryomilled (Ni + 0.5 wt pct AlN) powders was measured to be 44 μm, slightly larger than that of the conventional Ni powder but 9 μm smaller than the cryomilled Ni powder, and the median agglomerate size of the cryomilled (Ni + 2 wt pct AlN) powders drastically decreased to 17 μm.

During cryomilling, morphological and dimensional changes occurred not only with respect to the agglomerate, but also with respect to the second-phase, hard particles. After cryomilling the (Ni + AlN) powders, the AlN particles changed from their initial morphology as thin platelets[14,15] with an average size of 1.97 μm into very fine round particles with an average size of approximately 30 nm. Figures 3(a) and (b) show a uniform distribution of AlN particles (white particles) in the Ni matrix in the cryomilled (Ni + 0.5 wt pct AlN) powders. The TEM bright-field image of the cryomilled (Ni + 2 wt pct AlN) powder is shown in Figure 4(a), in which grain boundaries are not clearly visible. Using reflections from the AlN particle, the dark-field image in the corresponding field was taken, and the result is shown in Figure 4(b), indicating a consistent AlN particle size with those shown in Figure 3. Milling caused the Ni powder particles to continuously experience overlapping, welding, and fracturing as a result of the collisions between the powder and the milling media. In such a process, the fine, hard AlN particles impacted with the larger Ni agglomerates and were dispersively embedded into the Ni agglomerates.

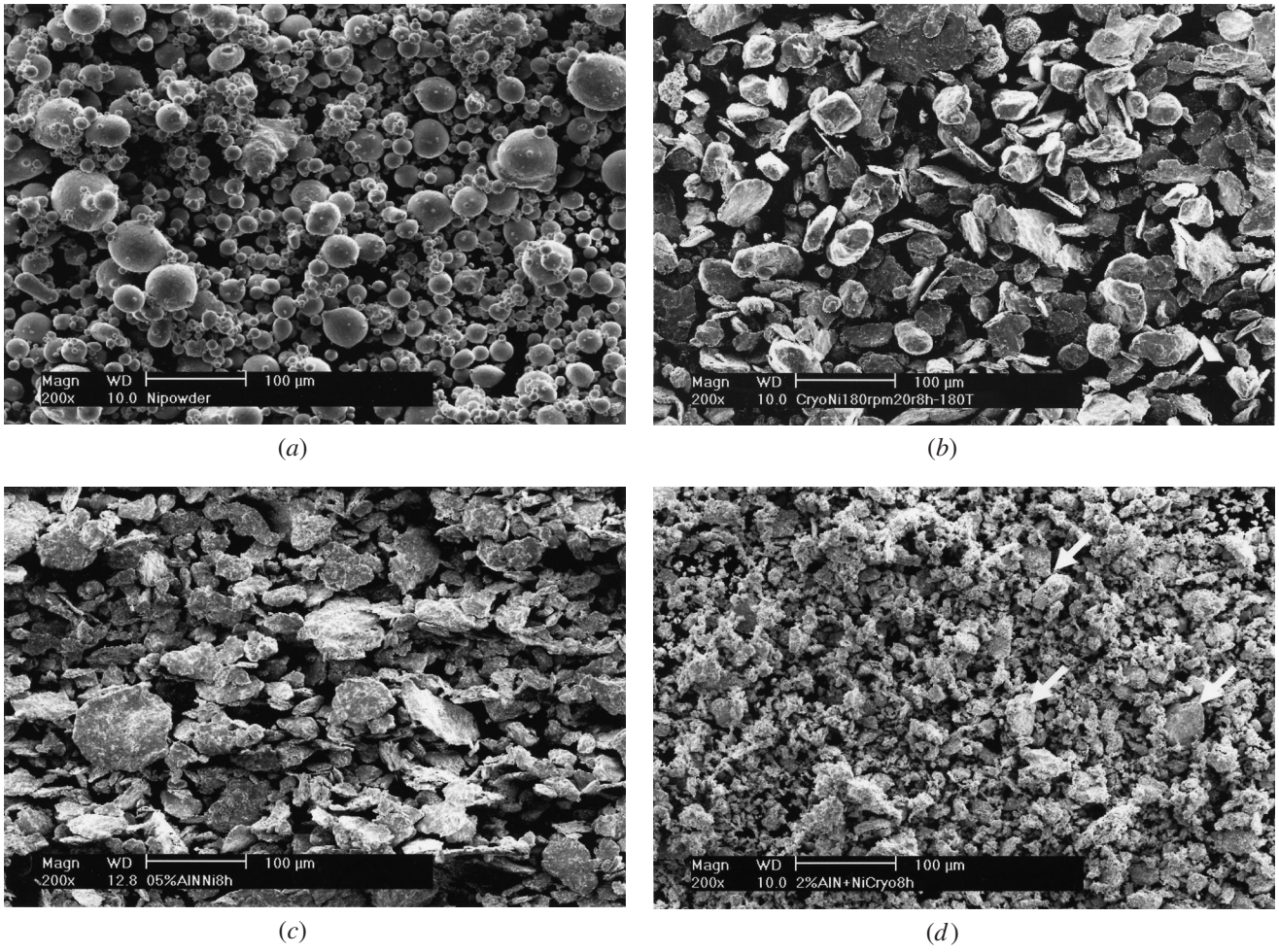

Fig. 1—SEM secondary electron images indicating morphology of powders. (*a*) The as-received Ni powders; (*b*) Ni powders cryomilled for 8 h at 100 K; (*c*) (Ni + 0.5 wt pct AlN) powders cryomilled for 8 h at 100 K; and (*d*) (Ni + 2 wt pct AlN) powders cryomilled for 8 h at 100 K (arrows indicate uncrushed agglomerates).

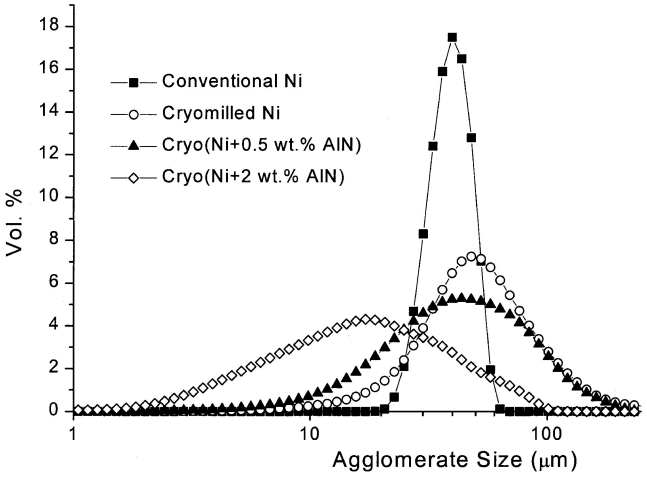

Fig. 2—Distribution of powder particle/agglomerate size. -■- conventional Ni powder with a median size of 41 μm; -○- cryomilled Ni powder with a median size of 53 μm; -▲- cryomilled (Ni + 0.5 wt pct AlN) powder with a median size of 44 μm; and -◇- cryomilled (Ni + 2 wt pct AlN) powder with a median size of 17 μm.

On the basis of reflection line broadening of XRD,[20,23] the grain size of the cryomilled Ni, cryomilled (Ni + 0.5 wt pct AlN), and cryomilled (Ni + 2 wt pct AlN) were calculated to be 105, 65, and 33 nm, respectively. These results indicate that the addition of hard AlN particles accelerated the formation of a nanocrystalline structure. In related studies, it was stated that the development of nanostructures in Zn and Cu-Ta systems during cryomilling evolved from the dynamic rearrangement of dislocations and recrystallization.[24,25] The steady-state grain sizes were achieved *via* the formation of new low-angle and then high-angle grain boundaries. The evolution of dislocation cell walls, the interpenetrating twin boundaries, the boundaries of deformation bands, or the nucleation and growth of new grains *via* dynamic recrystallization led to grain refinement. Sufficient energy stored in localized and highly strained regions caused by cryomilling induces or facilitates a recrystallization process in which new grains originate at the initial grain boundaries, but as the materials continue to be deformed, the dislocation density of the new grains increases, thus reducing the driving force for their further growth, and the recrystallizing grains eventually cease to grow. Therefore, grains remain in the nanometer dimension. Plastic damage occurs in the form of dislocations on the slip planes, whose density could exceed 10^{13} lines/cm^2. In the range of dislocation densities of 10^{13} to 10^{14}/cm^2, dislocation cores start to overlap and

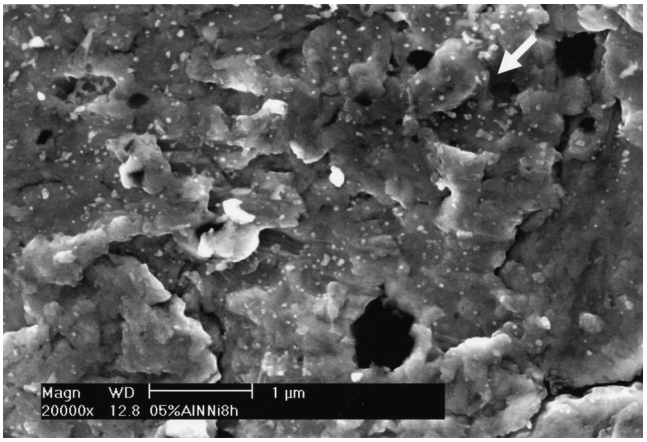

(*a*)

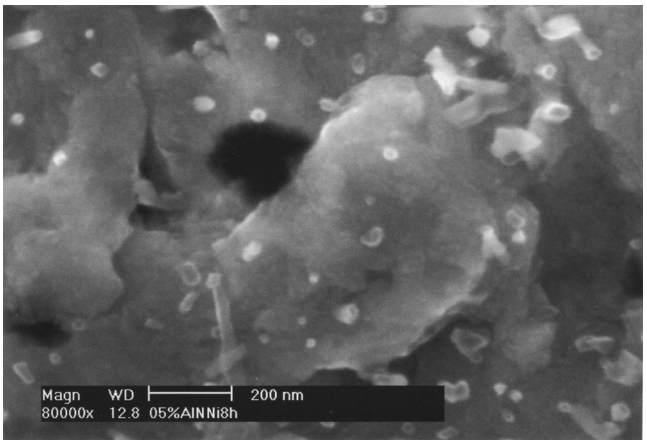

(*b*)

Fig. 3—Distribution of AlN particles in the cryomilled (Ni + 0.5 wt pct AlN) powders. (*a*) Distribution of AlN particles and (*b*) detailed view of the region indicated by the arrow in (a).

initialize dynamic recrystallization with small energy fluctuations.[24] In the present study, discontinuity of the crystal structure and the development of a heavy-strain field at the AlN/Ni interface lead to the emission and pileup of dislocations, thereby increasing the dislocation density significantly. Thus, the presence of hard particles accelerates grain refinement in the Ni matrix. Physical fragmentation of initial coarse grains could be an additional factor for improving the formation of a nanocrystalline structure by the addition of AlN particles. In a related study, the evolution of grains in the Ni-based superalloy INCONEL* 625 with increasing cryomilling time was investigated by TEM in detail.[22] The initial INCONEL 625 powder had equiaxed grains, and grains were elongated after cryomilling for 4 hours, similar to those observed in traditional cold-rolling/drawing materials. With increasing cryomilling time, powders experienced repeated fracturing,[26] and the elongated grains (having a high deformation-fault density) in the powders were sheared into nanosized fragments by cycling impact loading in random directions. In other words, physical fragmentation of highly deformed, initially coarse grains facilitated the formation of the nanocrystalline structure. It is also possible for hard AlN particles to assist this physical fragmentation of initially coarse grains and to promote the formation of a nanocrystalline structure in the Ni matrix, because the hard particles impact and partition the powder agglomerates into small fragments, as seen in Figure 1(d).

*INCONEL is a trademark of INCO Alloys International, Huntington Woods, WV.

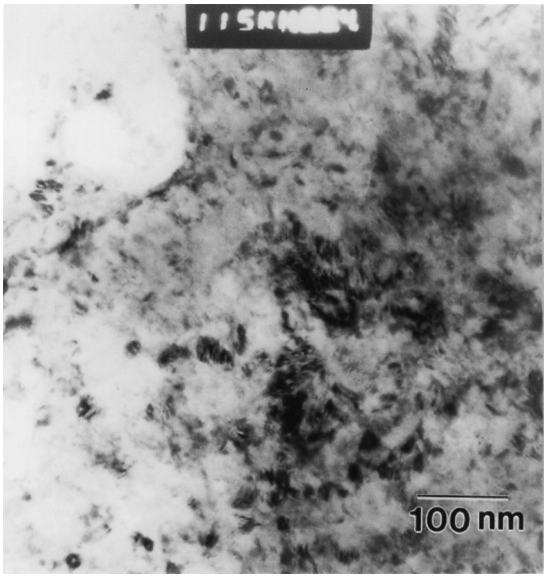

(*a*)

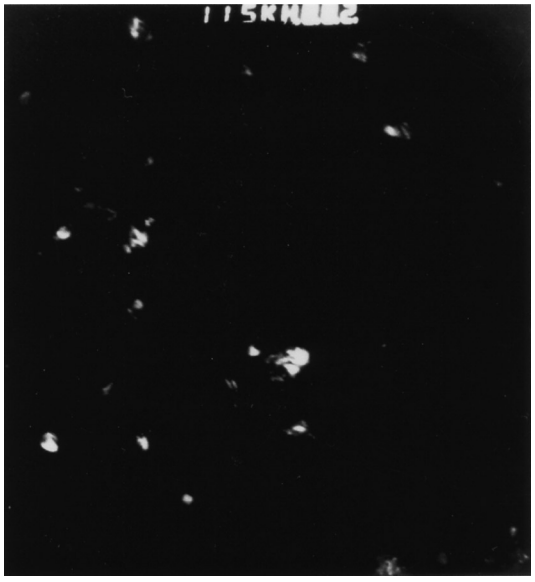

(*b*)

Fig. 4—TEM images of the cryomilled (Ni + 2 wt pct AlN) powder. (*a*) TEM bright-field image of cryomilled (Ni + 2 wt pct AlN) powder and (*b*) corresponding dark-field image using diffraction from AlN phase, indicating AlN particles.

The results of the chemical-composition analysis for the powders are listed in Table II. For comparison purposes, the nominal contents of aluminum and nitrogen for (Ni + AlN) powders, namely, aluminum and nitrogen resulting directly from the AlN phase itself, were calculated and are also incorporated in Table II. The results show that cryomilling leads to noticeable contamination. The increase in iron content resulted from the wear of the stainless steel milling tanks, shafts, and balls, which were severely worn by the powders containing hard particles. Neglecting the increase

Table II. Chemical Composition of the As-Received and Cryomilled Ni, Ni/AlN Powders (Weight Percent)

Code	Fe	Al	N	O	C
As-received Ni	0.02	0.01	0.02	0.48	0.014
Cryomilled Ni	0.08	0.03	0.05	0.51	0.034
Cryomilled (Ni + 0.5 wt pct AlN)/nominal	0.14	0.36/0.33	0.23/0.17	0.94	0.031
Cryomilled (Ni + 2 wt pct AlN)/nominal	0.36	1.37/1.32	0.90/0.68	1.17	0.054

in aluminum content coming directly from AlN, an evident net change in aluminum content is not observed. In general, the contents of nitrogen, oxygen, and carbon increased with increasing AlN content in the cryomilled powders. These elements originated from diffusion from the milling environments.[17,18,20,21] According to Table II, the net increase in nitrogen content is 0.06 and 0.32 wt pct for the cryomilled (Ni + 0.5 wt pct AlN) and the cryomilled (Ni + 2 wt pct AlN) powder, respectively. The presence of AlN particles also caused a noticeable increase in oxygen. The increased external surface areas in the cryomilled (Ni + AlN) powders, because of the rougher surface and smaller powder agglomerate size (Figures 1(c) and (d)), is the primary cause for the increase in the oxygen content and the net increase in nitrogen content.

B. *Microstructure and Mechanical Properties of the Coatings*

The SEM backscattered electron images in Figures 5(a) through (d) show the cross-sectional microstructures of the different coatings. The average coating thickness ranged from 230 to 260 μm. A noticeable difference between the microstructures, observed with SEM, of the conventional Ni, the cryo Ni, and the cryo (Ni + 0.5 wt pct AlN) coatings was not observed. The lamellar structure, which is typically observed in thermally sprayed coatings, and the lamellar-structure boundary which resulted as the surface of droplets solidified[27] are not clearly visible. However, the cryo (Ni + 2 wt pct AlN) coating (Figure 5(d)) exhibits a distinctive coarse lamellar structure at relatively low magnification. It is evident that the coarse lamellar structure corresponds to the spraying pass rather than the surface of droplets solidified. The five passes needed to make the coating are clearly seen, as a result of oxidation that occurred at the interpass boundaries (it can be seen from the distribution of oxygen shown in Figure 11).

The microstructures of the conventional Ni and the cryo Ni coatings were examined using TEM, and the results indicated that the majority of the grains in the cryo Ni coating were equiaxed, with an average grain size of 50 ± 23 nm.[12] The influence of the presence of AlN particles on the microstructure of the coatings was, therefore, investigated using TEM in the present study, and the results are shown in Figure 6. Figure 6(a) indicates a typical microstructure of the cryo (Ni + 2 wt pct AlN) coating. The majority of grains are also equiaxed, but with a much smaller average size of 24 ± 15 nm. Fine lamellar structures were observed in areas of the sample of approximately 10 pct (Figure 6(b)). The fine, equiaxed grains were observed in the areas between the lamellar structures. Approximately 20 pct of the sample area consisted of even-smaller equiaxed grains with an average size of 16 ± 10 nm, in which a large number of twins were present, shown in Figure 6(c). Mechanical twins are observed in the various cryomilled powders;[19,22] thus, the presence of twins in the coating is probably from the preservation of twins in the feedstock powders, and the related mechanism is discussed in detail elsewhere.[19]

In comparison with the microstructures of the cryo Ni coating, the following microstructural features were observed as a result of introducing 2 wt pct AlN particles into the Ni matrix: (1) a distinctive lamellar structure on SEM cross-sectional images, indicating that significant oxidation occurred at the interpass boundaries; (2) smaller grain sizes in the coatings, consistent with the smaller grain sizes in the cryomilled (Ni + 2 wt pct AlN) powder; and (3) the presence of twins in the cryo (Ni + 2 wt pct AlN) coatings.

The microhardness of the different coatings in cross section was tested with a load of 300 g, and the results are listed in Table III. The microhardness increased by only 6 pct in the cryo Ni coating, as compared to that of the conventional Ni coating. The addition of 2 wt pct AlN particles, however, led to an increase of approximately 60 pct, which is 10 times as large as the influence of cryomilling alone. Compared with the cryomilled Ni coating, the microhardness is increased by 18 and 47 pct for the cryo (Ni + 0.5 wt pct AlN) and the cryo (Ni + 2 wt pct AlN) coatings, respectively. It is universally accepted that both the grain refinement (*i.e.*, the Hall–Petch equation $H_v = H_0 + kd^{-1/2}$, where H_0 and k are constants and d is the diameter of the grain) and the presence of fine, hard, and dispersed particles (*i.e.*, References 1 through 3) lead to an increase in hardness. In the present study, both the grain refinement and the presence of fine, hard, and dispersed particles play a role in increasing hardness. On the basis of the Hall–Petch equation, the microhardness of the cryo (Ni + 2 wt pct AlN) coating was calculated to be 278, assuming approximate grain sizes of 100, 50,[12] and 24 nm (Figure 6(a)) for the conventional Ni, the cryo Ni, and the cryo (Ni + 2 wt pct AlN) coatings, respectively. This calculated value is much lower than the average measured value of 378. In fact, even the calculated value of 278 was an overly high estimated value, because the hardness of nanocrystalline materials has usually been observed to be lower than that predicted using the Hall–Petch equation.[28,29,30] Therefore, the results suggest that the major contribution to the increase in microhardness resulted from the addition of fine, hard, and dispersed particles.

Indentation-fracture performance is one of the most important mechanical properties for coatings. Anstis *et al.*[31] established a formula, $K_{IC} = 0.016\,(E/H)^{1/2}(P/c^{3/2})$, to calculate fracture toughness on the basis of mechanics analysis on the cracks caused by Vickers indentation. In this formula, P is the load, H is the Vickers microhardness of the coating, c is the crack length, E is the Young's modulus of the coating, and K_{IC} is the fracture-toughness value. The aforementioned model has been widely and directly applied to the calculation

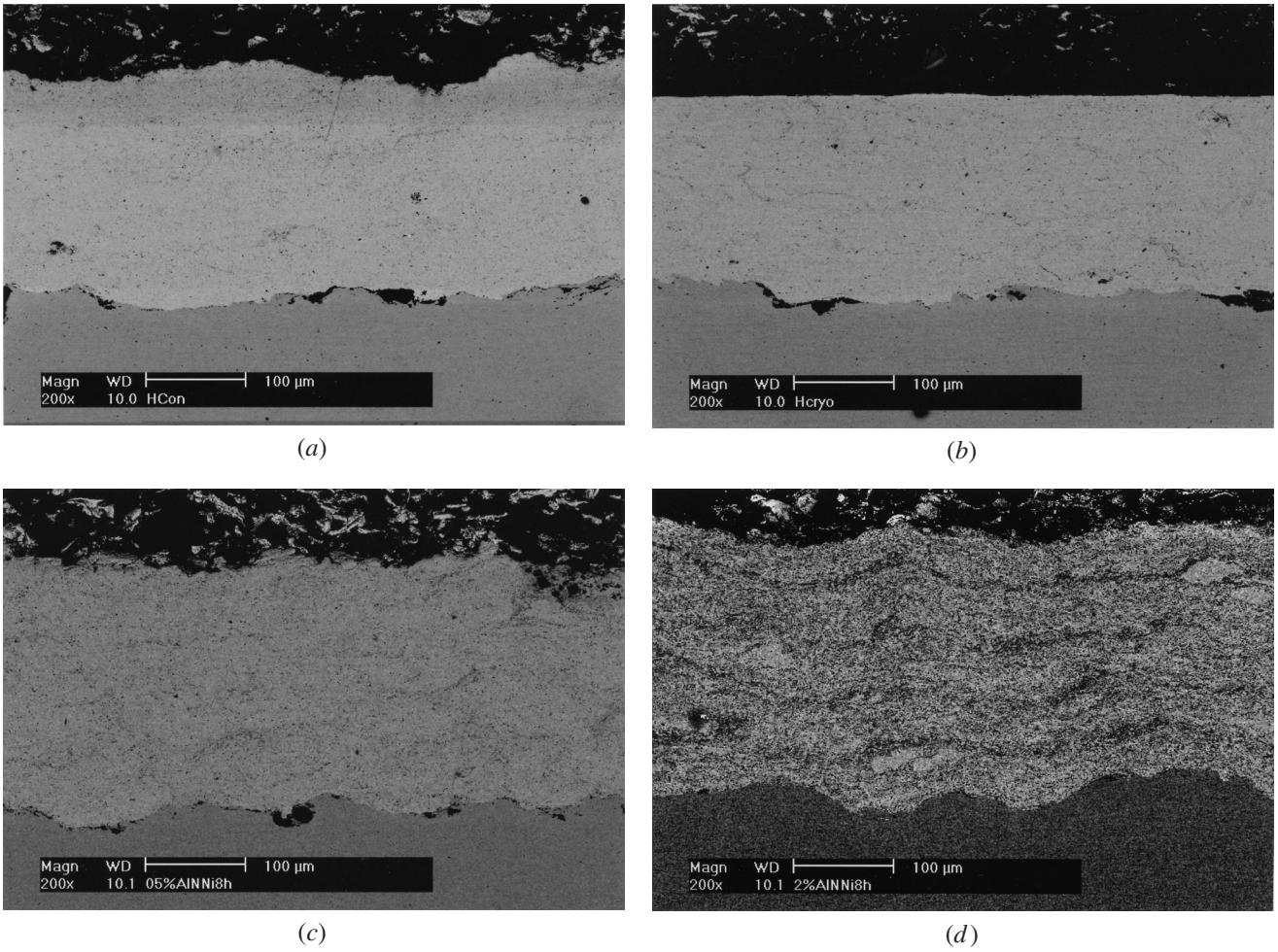

Fig. 5—SEM backscattered electron images of the different coatings produced using HVOF. (*a*) Cross section of the conventional Ni coating; (*b*) cross section of the cryo Ni coating; (*c*) cross section of the cryo (Ni + 0.5 wt pct AlN) coating; and (*d*) cross section of the cryo (Ni + 2 wt pct AlN) coating.

of fracture toughness of thermally sprayed coatings,[32,33] regardless of the isotropic-structure requirement of the model.[31] However, thermally sprayed coatings have an anisotropic microstructure, *e.g.*, the Young's modulus of plasma-sprayed WC-12 wt pct Co coatings parallel to the coating plane was reported to be about twice as large as that perpendicular to it.[34] In a material having an isotropic microstructure, four symmetrical indentation cracks were observed on the extended lines of the diagonals related to the quadrilateral pyramid indentation, where a maximum stress concentration caused by indentation is present.[31] However, in thermally sprayed coatings, indentation cracks usually appear in the direction parallel to the coating plane. In addition, cracks are not present directly on the extended line of the diagonal of the indentation. Instead, indentation cracks on the cross section of thermally sprayed coatings result from a stress-field interaction with large pores or defects located near the impression diagonals. There are no cracks in the direction perpendicular to the coating plane.[17,18] The presence of a preferred direction for crack initiation and propagation is attributed to the thermal-spray process. A complete coating is gradually produced by passing the thermal-spray torch across the substrate several times. Because each layer had once been the outer surface, there is a potential for contamination to occur and to become covered by the next layer. Moreover, at layer boundaries, a discontinuity in the heat and mass transfer may have led to a discontinuity in the behavior of coatings. Therefore, thermally sprayed coatings have different structures and properties when parallel to or perpendicular to the coating plane. On the basis of the previous arguments, the fracture-toughness value obtained by the formula $K_{IC} = 0.016\ (E/H)^{1/2}(P/c^{3/2})$ is considered as a relative fracture toughness in the direction perpendicular to the coating plane (perpendicular to the crack-propagation plane). For the present coatings, under a 1000 g load, the microhardness and crack length were measured from an average reading of 5 tests. The Young's modulus of all Ni/AlN coatings is estimated to be about 103 GPa,[35] and the relative fracture-toughness values were obtained at $K_{IC} = 0.016\ (E/H)^{1/2}(P/c^{3/2})$ and are also listed in Table III. The addition of AlN particles increased the relative fracture-toughness value.

To indicate the influence of the addition of AlN particles on fracture toughness, illustrative indentation-crack configurations are shown in Figures 7(a) through (d). Under the same load, indentation marks in the cryo (Ni + 2 wt pct AlN) coating are smaller than those in the conventional Ni coating, because the former has a higher hardness than the latter. Under a load of 500 g, a crack, located far away from the indentation as shown by the white arrow, was present in the conventional Ni coating. No cracking was observed around the indentation in the cryo (Ni + 2 wt pct AlN)

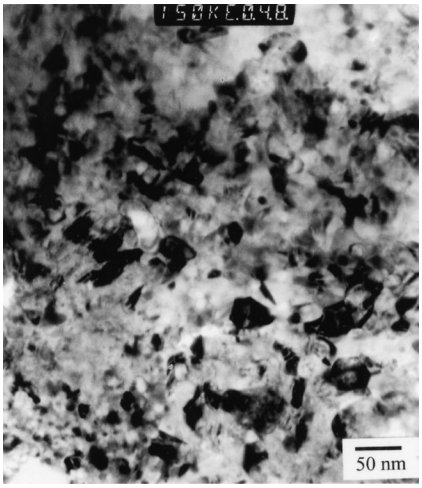

(*a*)

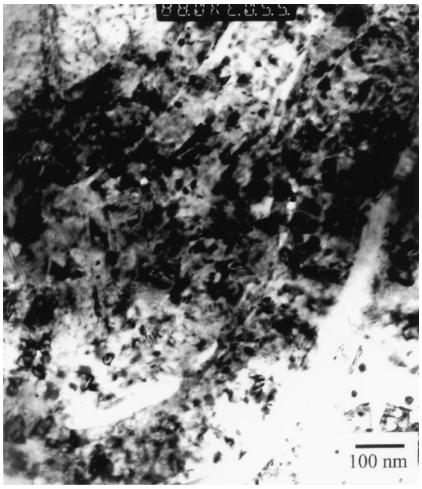

(*b*)

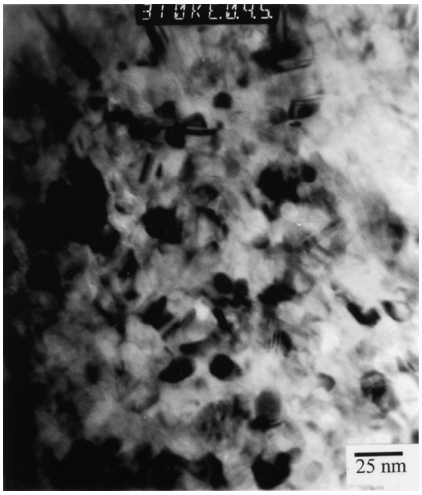

(*c*)

Fig. 6—TEM images of the cryo (Ni + 2 wt pct AlN) coating. (*a*) TEM bright-field image; (*b*) lamellar structure; and (*c*) fine grains with a number of twins.

coating. Under a load of 1000 g, many cracks near the indentation, and even delamination of the coating, were observed in the conventional Ni coating. In contrast, only a short crack was observed in the cryo (Ni + 2 wt pct AlN) coating. Therefore, the present results suggest that the cryo (Ni + 2 wt pct AlN) coating possessed a higher fracture toughness relative to that of the conventional Ni coating. It is well known that both the strength/hardness and ductility of conventional materials increases as the grain size decreases. It is reported that the nanocrystalline Al alloy exhibits superplasticity at a relatively high strain rate.[36] Therefore, grain refinement of the Ni matrix caused by the addition of AlN particles might result in the increase in the relative fracture toughness in the cryo (Ni + AlN) coatings. In addition, the characteristics of the feedstock powder, *i.e.*, the morphology and dimensions of the powder, affect the temperature that the powder experiences during HVOF spraying and, hence, modify coating the toughness by influencing the solidification and oxidation process of splats sprayed on the substrate.[27] Smaller powder particles lead to a higher powder temperature. The porosity in the coatings depends primarily on the temperature that the powder experiences during spraying, and the higher the powder temperature, the lower the porosity in the coatings and the higher the wear resistance.[37,38] Thus, unique characteristics of the agglomerate size of the (Ni + 2 wt pct AlN) powder may benefit the achievement of coatings having a high fracture toughness.

Table III. Average Microhardness and Relative Fracture Toughness of the Ni/AlN Coatings

Code	Conventional Ni	Cryo Ni	Cryo (Ni + 0.5 Wt Pct AlN)	Cryo (Ni + 2 Wt Pct AlN)
Hardness (HV_{300})	243	258	304	378
Increase in hardness (percent)	NA	6	25	59
K_{IC} (MPa$\sqrt{m}$)	13	14	16	17

C. *Identification of Particle Phase in Coatings*

The XRD spectra for the four coatings, as well as for the cryomilled (Ni + 2 wt pct AlN) powders, are shown in Figure 8. In order to analyze the hard-particle phases with low volume fraction in the coatings, a very slow scan rate of 0.12 deg/min was employed when the XRD experiments were carried out. Even so, AlN particles were not detected in any of the coatings. Moreover, distinctive reflections from the AlN phase were also not observed in the X-ray spectrum for the cryomilled (Ni + 2 wt pct AlN) powder, although SEM and TEM observations indicate a uniform distribution of AlN particles in the cryomilled (Ni + AlN) powders (Figures 3 and 4). The failure to detect AlN particles by using XRD does not indicate the absence of AlN particles in the coatings. AlN exhibits a melting point of approximately 2800 °C[39] and is thermally stable up to 2200 °C,[40] much higher than the temperatures of 1300 °C to 1900 °C that powders experience during thermal spraying.[27] Thus, it is presumed that AlN particles were stable during thermal spraying. However, AlN powder is unstable in moist air and releases an ammonia odor.[14] Thermodynamically, the hydrolysis reaction $2AlN + 3H_2O = 2NH_3 + Al_2O_3$ is possible because the free energy (ΔG) of the reaction at

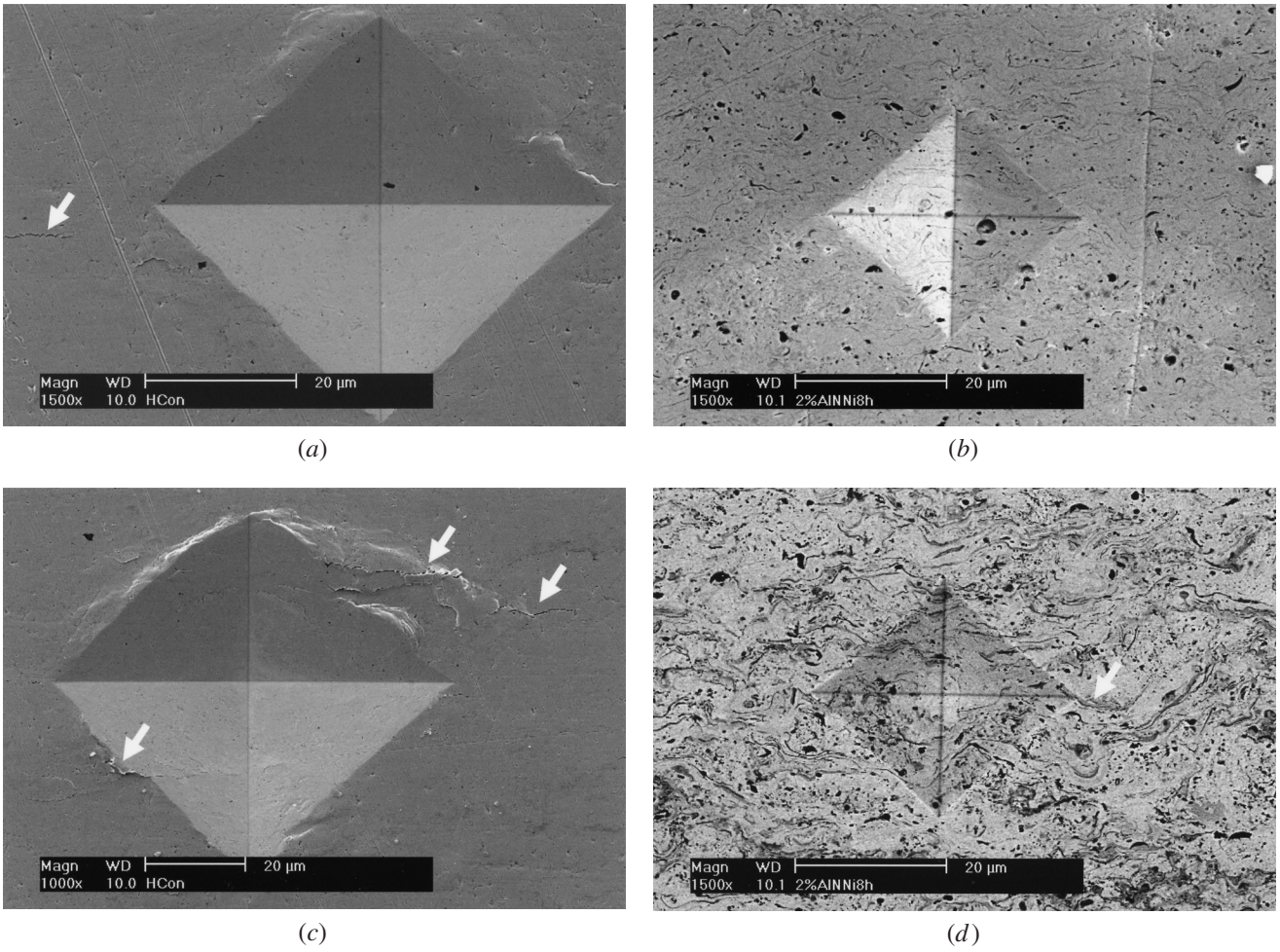

Fig. 7—Indentation cracking in coatings. Arrows indicate cracking. (*a*) Conventional Ni coating at 500 g; (*b*) cryo (Ni + 2 wt pct AlN) coating at 500 g; (*c*) conventional Ni coating at 1000 g; and (*d*) cryo (Ni + 2 wt pct AlN) coating at 1000 g.

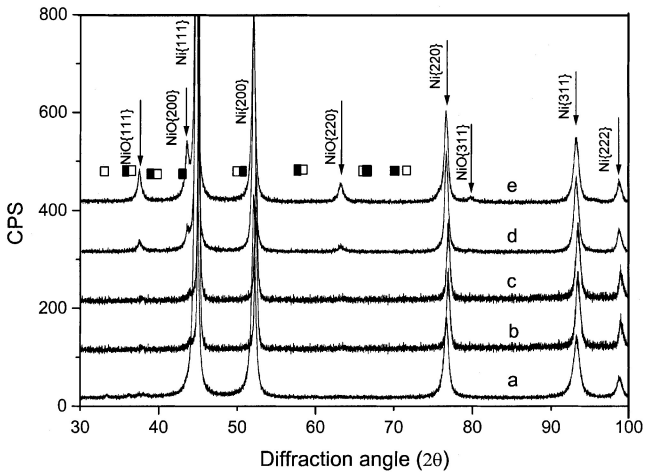

Fig. 8—XRD spectra for coatings and cryo (Ni + 2 wt pct AlN) powder. The symbols □ and ■ indicate the angle where the reflections of AlN and Al_2O_3 phases would be, respectively. (*a*) Cryomilled (Ni + 2 wt pct AlN) powder; (*b*) conventional Ni coating; (*c*) cryomilled Ni coating; (*d*) cryo (Ni + 0.5 wt pct AlN) coating; and (*e*) cryo (Ni + 2 wt pct AlN) coating.

300 K is calculated to be −332.4 kJ, on the basis of the thermodynamic data,[13] and a related study confirmed the hydrolysis of AlN powder in aqueous environments.[41] In fact, an ammonia odor was detected when the cryomilled (Ni + AlN) powders were sampled. Therefore, it is believed that a trace amount of AlN has decomposed, even though Al_2O_3 was also not detectable by XRD (the angles where the reflections of Al_2O_3 would be also are indicated in Figure 8). It is commonly known that a small amount of light elements (low Z) in a heavy-element (high Z) matrix are invisible due to the absorption of the X-rays.[42] The intensity of a reflection is proportional to the square of the atomic scattering factor (f) of the diffracted material. The atomic scattering factors of aluminum (the values for AlN and Al_2O_3 are not available) and nickel are listed in Table IV.[42] In addition, the AlN and Al_2O_3 have nanometer sizes and, hence, extensively broadened diffraction peaks that are difficult to be observed.

The presence of NiO phase was confirmed by XRD. Only traces of NiO phase were detected in the conventional Ni and the cryo Ni coatings. In the cryo (Ni + 0.5 wt pct AlN) and the cryo (Ni + 2 wt pct AlN) coatings, 1.3 and 4.1 vol pct NiO was detected, respectively. Only a trace of NiO was detected in the cryomilled (Ni + 2 wt pct AlN) powders, indicating that the NiO observed in the coatings primarily formed during thermal spraying. The oxidation process occurs rapidly in the presence of oxygen in the surrounding air and/or excess oxygen during HVOF spraying; particles

Table IV. Atomic Scattering Factors (f) of Nickel and Aluminum

Sin θ/λ (A^{-1})	0.0	0.1	0.2	0.3	0.4	0.5	0.6	0.7	0.8	0.9	1.0
Ni	28.0	25.0	20.7	17.2	14.6	12.7	11.2	9.8	8.7	7.7	7.0
Al	13.0	11.0	8.95	7.75	6.6	5.5	4.5	3.7	3.1	2.65	2.3

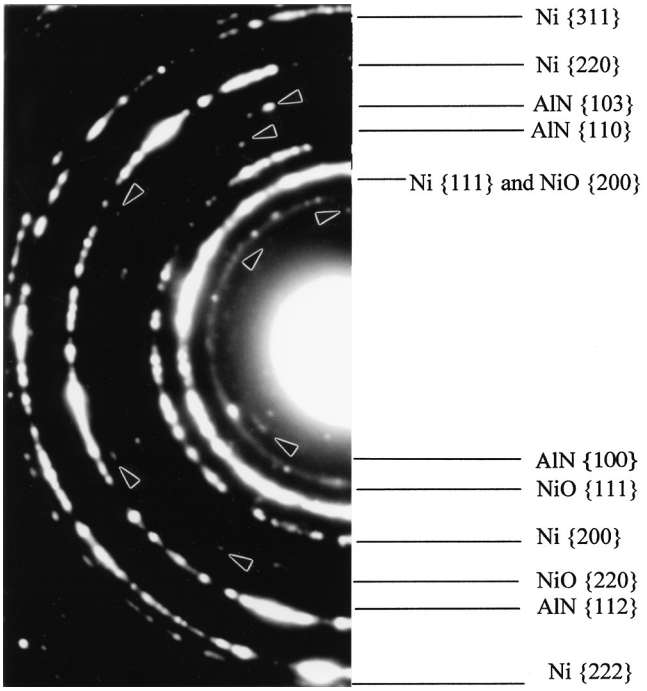

Fig. 9—TEM selected-area diffraction pattern of cryo (Ni + 2 wt pct AlN) coating; the arrows indicate diffraction spots from AlN.

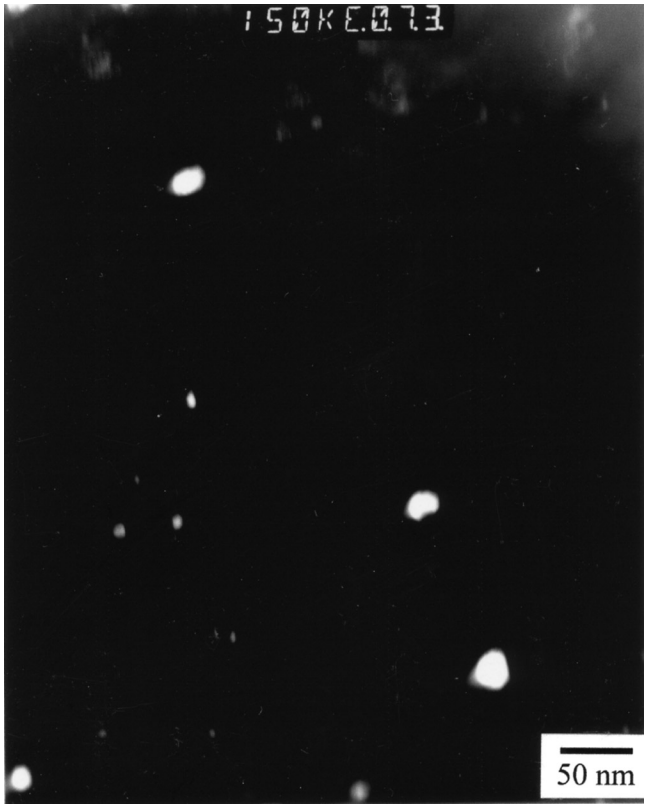

Fig. 10—TEM dark-field image of cryo (Ni + 2 wt pct AlN) coating taken by using $\{111\}_{NiO}$, indicating NiO particles.

exposed to high temperature can oxidize during in-flight and after impingement onto the substrate surface.[43] The formation of an oxide layer comprises the complex processes of adsorption of oxygen molecules on the material surface, dissociation of the oxygen molecules, formation of oxide nuclei, and, finally, the growth of nuclei to form a complete oxide layer.[44] Therefore, the amount of oxide formed during HVOF spraying depends on the oxygen concentration at the particle surface, the free specific surface area of the particles, and the temperature and time that the particles are exposed to oxygen. Because of the increased external surface area and higher oxygen content (Table II) of the (Ni + AlN) powders, as well the fact that small agglomerates experience higher temperatures than do large agglomerates during thermal spraying,[27] it is not surprising that the volume fraction of the NiO phase increased with increasing amounts of the AlN particles.

The TEM selected-area diffraction pattern, corresponding to the bright-field image shown in Figure 6(a), with its index is shown in Figure 9. The diffraction patterns from the AlN phase were imaged and are indicated by the arrows. The diffraction patterns from the AlN phase were quite weak and very close to those from the Ni matrix and NiO phase, and the strongest diffraction of $\{100\}_{AlN}$ was covered in the range of the illumination from the central transmission spot. This led to unsuccessful attempts to take dark-field images of the AlN phase with the purpose of exhibiting the dimensions and the distribution of particles. Using the $\{111\}_{NiO}$ reflection, a dark-field image was taken and is shown in Figure 10. The result indicates that the NiO phase existed in the form of round particles, the bigger ones approximately 30 nm in size and the smaller ones less than 10 nm. To disclose the features of the particles, SEM X-ray elemental dot mapping was performed to show the distributions of oxygen and aluminum on the cross section of the cryo (Ni + 2 wt pct AlN) coating. The results, shown in Figure 11, indicate that the deep-gray contrast strips at boundaries of interpassing can be rationalized by the presence of oxides. It is, however, noted that the oxides were present throughout the coating. Aluminum is homogeneously distributed throughout the coating, indicating the presence of AlN particles in the cryo (Ni + 2 wt pct AlN) coating. Therefore, it is reasonably assumed that the cryo (Ni + 2 wt pct AlN) coating consists of ~5 vol pct AlN, ~4 vol pct NiO, a trace amount of Al_2O_3, and the balance Ni.

IV. CONCLUSIONS

In the present study, nanocrystalline Ni powders containing ultrafine AlN particles were synthesized by using

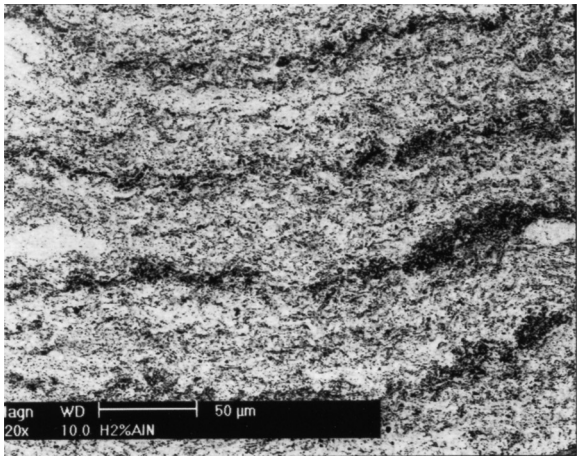

(*a*)

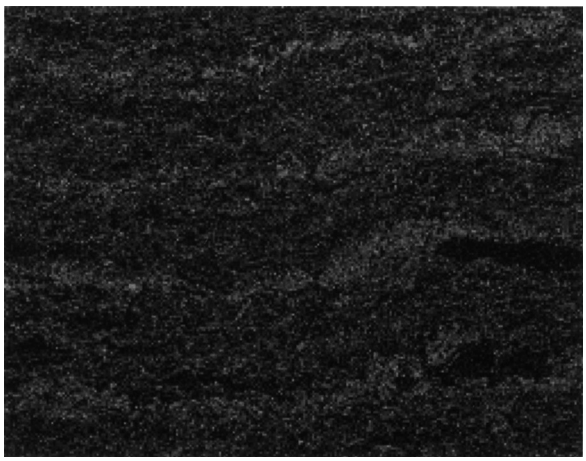

(*b*)

(*c*)

Fig. 11—Distributions of oxygen and aluminum on cross section of the cryo (Ni + 2 wt pct AlN) coating. (*a*) SEM secondary electron image; (*b*) X-ray mapping of oxygen; and (*c*) X-ray mapping of aluminum.

cryomilling. The resultant powders were employed as feedstock powders to fabricate hard-particle-strengthened nanocrystalline Ni coatings. The results are briefly summarized as follows.

1. The ability to introduce a secondary nitride phase into Ni using AlN additions has been successfully demonstrated. The presence of this secondary phase led to improved mechanical behavior in HVOF coatings, as desired and predicted.
2. The AlN additive was reduced in size from a starting powder size of 2 μm to ultrafine particles of approximately 30 nm in diameter. These particles were dispersively embedded into the Ni matrix and enhanced the development of a nanocrystalline structure in the Ni matrix during cryomilling.
3. The presence of AlN particles in the powders decreased the agglomerate size and increased the surface roughness of the agglomerates.
4. The addition of AlN also led to an increase in the amount of NiO phase that was distributed in the coatings in the form of ultrafine, round particles.
5. A decreased grain size was achieved in the AlN-strengthened Ni coating, compared to the cryo Ni coatings. Smaller initial grains in the feedstock powder caused by the addition of AlN and the increase in the amount of the dispersed, ultrafine particles (AlN and NiO) that inhibit grain growth were attributed to the observed smaller grain size in the AlN-strengthened Ni coating.
6. Compared with that of the cryomilled Ni coating, an increase in microhardness by 18 and 47 pct was obtained for the additions of 0.5 and 2 wt pct AlN, respectively. Indentation-fracture results also indicated that the fine, dispersed AlN particles raised the apparent toughness of the Ni coating. The increase in microhardness resulted from both grain refinement and the presence of ultrafine particles. However, the latter played the primary role in strengthening.

ACKNOWLEDGMENTS

The authors thank Drs. K.H. Chung and L. Ajdelsztajn, University of California, Davis, for their assistance with the cryomilling and thermal spraying experiments. The authors also gratefully acknowledge financial support provided by the Office of Naval Research under Grant Nos. N00014-98-01-0569, and N00014-01-C-0384.

REFERENCES

1. N.F. Mott and F.R.N. Nabarro: *Proc. Phys. Soc.*, 1940, vol. 52, p. 86.
2. E. Orowan: *Symp. on Internal Stress in Metals and Alloys: Session III Discussion*, Institute of Metals, London, 1948, p. 451.
3. A.J. Ardell: *Metall. Trans. A*, 1985, vol. 16A, pp. 2131-65.
4. C.S. Smith: *Trans. AIME*, 1948, vol. 175, pp. 15-51.
5. D.G. Morris and M.A. Morris: *Acta Metall. Mater.*, 1991, vol. 39, pp. 1763-70.
6. M.J. Luton, C.S. Jayanth, M.M. Disco, S. Matras, and J. Vallone: in *Multicomponent Ultrafine Microstructures*, L.E. McCandlish, B.H. Kear, D.E. Polk, and R.W. Siegel, eds., Materials Research Society, Pittsburgh, PA, 1989, pp. 79-86.
7. R.J. Perez, H.G. Jiang, C.P. Dogan, and E.J. Lavernia: *Metall. Mater. Trans. A*, 1998, vol. 29A, pp. 2469-75.
8. B. Huang, J. Vallone, and M.J. Luton: *Nanostr. Mater.*, 1995, vol. 5, pp. 631-42.
9. J.D. Whittenberger and M.J. Luton: *J. Mater. Res.*, 1995, vol. 10, pp. 1171-86.
10. J. He and E.J. Lavernia: *Mater. Sci. Eng. A*, 2001, vol. A 301, pp. 69-79.
11. J. He, M. Ice, J.M. Schoenung, D.H. Shin, and E.J. Lavernia: *J. Thermal Spray Technol.*, 2001, vol. 10, pp. 293-300.
12. M.L. Lau, J. He, A.J. Melmed, T.A. Lusby, R. Schweinfest, M. Ruhle, and E.J. Lavernia: *J. Mater. Res.*, 2002, vol. 17, pp. 1041-49.
13. E.A. Brands and G.B. Brook: *Smithells Metals Reference Book*, 7th

ed., Butterworth-Heinemann, Oxford, United Kingdom, 1992, pp. 8:23-8:26.
14. Certificate of Analysis comes with the AlN powder, CERAC Inc., Milwaukee, WI, 2001.
15. F.G. Wilson and T. Gladman: *Int. Mater. Rev.*, 1988, vol. 33, pp. 221-86.
16. M.L. Bauccio: *Metals Reference Book*, 3rd ed., ASM INTERNATIONAL, Materials Park, OH, 1999, p. 153.
17. J. He, M. Ice, S. Dallek, and E.J. Lavernia: *Metall. Mater. Trans. A*, 2000, vol. 31A, pp. 541-53.
18. J. He, M. Ice, and E.J. Lavernia: *Metall. Mater. Trans. A*, 2000, vol. 31A, pp. 555-64.
19. J. He, K.H. Chung, X. Liao, Y.T. Zhu, and E.J. Lavernia: *Metall. Mater. Trans. A*, 2003, vol. 34A, pp. 707-12.
20. J. He, L. Ajdelsztajn, and E.J. Lavernia: *J. Mater. Res.*, 2001, vol. 16, pp. 478-88.
21. J. He, M. Ice, and E.J. Lavernia: *Nanostr. Mater.*, 1998, vol. 10, pp. 1271-83.
22. J. He and E.J. Lavernia: *J. Mater. Res.*, 2001, vol. 16, pp. 2724-32.
23. H.P. Klug and L.E. Alexander: *X-ray Diffraction Procedures*, John Wiley & Sons, New York, NY, 1974, p. 643.
24. X. Zhang, H. Wang, J. Narayan, and C.C. Koch: *Acta Mater.*, 2001, vol. 49, pp. 1319-26.
25. J. Xu, J.H. He, and E. Ma: *Metall. Mater. Trans. A*, 1997, vol. 28A, pp. 1569-80.
26. J.S. Benjamin: *Metall. Trans.* 1970, vol. 1, pp. 2943-51.
27. J. He, M. Ice, and E.J. Lavernia: *J. Thermal Spray Technol.*, 2000, vol. 10, pp. 83-93.
28. X.D. Liu, M. Nagumo, and M. Umemoto: *Mater. Trans., JIM*, 1997, vol. 38, pp. 1033-39.
29. C. Suryanarayana, D. Mukhopadhyay, S.N. Patankar, and F.H. Froes: *J. Mater. Res.*, 1992, vol. 7, pp. 2114-17.
30. D.A. Konstantinidis and E.C. Aifantis: *NanoStructured Mater.*, 1998, vol. 10, pp. 1111-18.
31. G.R. Anstis, P. Chantikul, B.R. Lawn, and D.B. Marshall: *J. Am. Ceram. Soc.* 1981, vol. 64, pp. 533-38.
32. V. Fervel, B. Normand, and C. Coddet: *Wear*, 1999, vol. 230, pp. 70-77.
33. H. Li, K.A. Khor, and P. Cheang: *Surf. Coating Technol.*, 2002, vol. 155, pp. 21-32.
34. H. Nakahira, K. Tani, K. Miyajima, and Y. Harada: *Proc. Int. Thermal Spray Conf. Exp.*, Orlando, Fl, May 28–June 5, 1992, C.C. Berndt, ed., ASM International, Materials Park, OH, 1992, pp. 1011-17.
35. T. Gnaupel-Herold and H.J. Prask: *Annual Report*, 2000, National Institute of Standards and Technology, United States Department of Commerce, Gaithersburg, MD, pp. 28-29.
36. R.S. Mishra, M.W. Mahoney, S.X. McFadden, N.A. Mara, and A.K. Mukherjee: *Scripta Mater.*, 2000, vol. 42, pp. 163-68.
37. J. He, Y. Liu, Y. Qiao, T.E. Fischer, and E.J. Lavernia: *Metall. Mater. Trans. A*, 2002, vol. 33A, pp. 145-57.
38. Y. Liu, Y. Qiao, J. He, E.J. Lavernia, and T.E. Fischer: *Metall. Mater. Trans. A*, 2002, vol. 33A, pp. 159-64.
39. H.A. Wriedt: in *Binary Alloy Phase Diagrams,* 2nd ed., T.B. Massalski, ed., ASM INTERNATIONAL, Materials Park, OH, 1990, p. 176.
40. F. Benesovsky: in *Encyclopedia of Chemical Technology*, 3rd ed., M. Grayson, ed., John Wiley & Sons, New York, NY, 1978, vol. 15, p. 876.
41. S. Novak and T. Kosmac: *J. Mater. Res.*, 2002, vol. 17, pp. 445-50.
42. B.D. Gullity: *Elements of X-ray Diffraction*, Addison-Wesley Publishing Co., Inc., Reading, MA, 1959, p. 474.
43. V.V. Sobolev, J.M. Guilemany, J. Nutting, and J.R. Miquel: *Int. Mater. Rev.*, 1997, vol. 42, pp. 117-36.
44. P. Scharwaechter, M. Wimmer, R. Wurschum, D. Plachke, and H.D. Carstanjen: *Nanostr. Mater.*, 1999, vol. 11, pp. 37-42.